**SUPPORTING INFORMATION**

# Theoretical study of the $O(^3P) + SiH_4$ reaction: Global potential energy surface, kinetics and dynamics study.

C. Rangel and J. Espinosa-Garcia*

*E-mail: joaquin@unex.es

## 1. Test of quality of PES-2022. Comparison with the input data

Table 1 shows the stationary point properties (geometry, vibrational frequencies and energies) obtained with PES-2022, together with the *ab initio* data for comparison. The reactants and products properties are well reproduced, where the $SiH_4$ and $SiH_3$ present $T_d$ and $C_{3v}$ symmetry, respectively. *Ab initio* and PES-2022 vibrational frequencies present a linear regression, $f_{PES}$ = a. $f_{ab\ initio}$ + b, with $R^2$> 0.99. The classical energy of reaction, $\Delta E_R$, and the standard enthalpy of reaction, $\Delta H_R$(298 K), are well reproduced, with differences lower than 0.2 kcal mol$^{-1}$, the latter being in excellent agreement with the experimental value[21] from the standard enthalpies of formation, -10.45 kcal mol$^{-1}$.

The saddle point requires accurate description because it represents a sensitive zone of the surface, related with the curvature of the reaction path, and thus with the tunneling contribution. Again, the *ab initio* and PES-2022 vibrational frequencies are linearly correlated, with a coefficient $R^2$ = 09937, the imaginary frequency presenting a larger difference, 1309 i versus 1103 i cm$^{-1}$. Therefore, the crossover temperature decreases from 300 K to 253 K. The length of the formed H-O and broken Si-H bonds are 1.303 and 1.570 Å, respectively, simulating the *ab initio* information, 1.363 and 1.599 Å. With PES-2022, these lengths increase by 34 and 6%, respectively, with respect to the products and reactants, and so this stationary point can be catalogued as an ‘‘early’’ transition state, in consonance with the exothermicity of the title reaction. The classical barrier height, $\Delta E^{\neq}$ = 5.18 kcal mol$^{-1}$ reproduces the *ab initio* data, 5.35 kcal mol$^{-1}$.

The reaction path comparison is shown in Figure 1, and it represents a second test of quality of the PES. The new surface reasonably simulates the topography of the reaction path, with a root-mean-square error (RMSE) of 0.50 kcal mol$^{-1}$. It is well known that kinetics (tunneling effect) and dynamics (for instance, translational,

rotational and vibrational distributions in the products) properties depend on the topography of the reaction path.

The energy dependence of the Si–H–O bonding angle in the saddle point for PES-2022 and the CCSD(T)/cc-pVTZ level is plotted in Figure S1, which represents the third test. We observed differences of only 0.2 kcalmol$^{-1}$ for separations of linearity of 20º, which increases to 1.4 kcal mol$^{-1}$ for separations of 40º. Schatz et al. (Ref. s1,s2) suggested that these deviations have dynamics consequences, so that hotter product rotational distributions are related with looser saddle points. However, this is not the only reason (and sometimes it is not the main reason) to obtain hot product rotational distributions, as analyzed in our previous study F($^2$P) + $SiH_4$ reaction,[3] where hot rotational distributions were associated to QCT limitations.

This section finishes with another stringent test of quality of the new surface. A two-dimensional equipotential contour plot for PES-2022 is shown in Figure S2, which represents the evolution of the broken and formed Si–H and O–H, bonds. A continuous and smooth surface is clearly observed, free of spurious minima, i.e., unphysical features.

Finally, note that as PES-2022 is fitted to the input data, these comparisons must therefore be considered merely as a self-consistent test.

**2. Kinetics computational details**

Based on the PES-2022 surface, the rate constants were calculated using the variational transition-state theory with multidimensional tunnelling corrections (VTST/MT), which permits to analyse tunnelling and recrossing effects at low computational cost (if an analytical surface is available).

In its canonical version, CVT,[s3,s4] the thermal rate constants in the range 300-1000 K (for a direct comparison with experiments, although a wider range can be easily obtained) were calculated as,

$$k^{CVT}(T) = \sigma \frac{k_B T}{h} K^o \min_s \exp\left[\frac{-\Delta G^{GT,o}(T, s^{*,CVT})}{k_B T}\right] \qquad \text{(S1)}$$

$k_B$, T, h and K$^o$ being, respectively, Boltzmann constant, temperature, Planck constant and reciprocal of the standard-state concentration, 1 molecule cm$^3$, and σ represents the symmetry factor or number of equivalent paths, four for the forward reaction. The reaction coordinate, s, is varied until the maximum of the free energy of activation, ΔG,

is reached, which corresponds to the dividing surface $s^{*,CVT}$. In order to obtain ΔG, the rotational partition functions were calculated classically and the vibrational partition functions were calculated as harmonic oscillators using redundant internal coordinates.[s5-s7] The electronic partition function ratio between the saddle point and the reactant, O($^3$P), is included in the rate constants calculation as,

$$Q_e(T) = \frac{6}{5 + 3exp(-E(3P_1)/RT) + exp(-E(3P_0)/RT)} \quad \text{(S2)}$$

In the numerator, the number 6 is a consequence of the triplet state in the transition state and of the presence of the two practically degenerate $^3$A' y $^3$A'' surfaces. In the denominator, we consider the O($^3$P) reactant electronic partition function, with $E(^3P_1)$ and $E(^3P_0)$ being the energies of the upper spin–orbit levels relative to its electronic ground state (158.29 and 226.99 cm$^{-1}$, respectively).

Finally, the tunneling correction was calculated using the microcanonical optimized multidimensional tunnelling approach, μOMT.[s8] A priori, given the heavy-light-heavy mass combination, this reactive system is good for presenting tunneling effects, especially at low temperatures. However, when zero-point energies are included, the adiabatic barrier is low, 1.83 kcal mol$^{-1}$ (versus 5.18 kcal mol$^{-1}$ for the classical barrier) and so the tunneling factor is likely to be small. All kinetics calculations were performed using the Polyrate-2016 code[s9].

**3. Dynamics computational details**

As noted previously in Introduction, two different series of experimental dynamics results were reported: at room temperature[6] and at collision energy[20] of 8.0 kcal mol$^{-1}$. In order to simulate these experiments, quasi-classical trajectory (QCT) calculations based on the PES-2022 surface were independently performed in these conditions, T=298 K and E=8.0 kcal mol$^{-1}$, using the VENUS code.[s10,s11] We begin by describing the initial conditions. In each case, two million trajectories were run with a propagation step of 0.1 fs, and a Si-O separation fixed at 15.0 Å to ensure reactant and product asymptotes with no interaction. In the calculations at T=298 K, translational, rotational and vibrational energies of reactants were selected by thermal sampling at this temperature, while in the calculations at fixed energy, the experimental conditions were

simulated with silane cold rotational energy (10 K) and vibrational ground-state. In both series, the remaining initial conditions were selected from a Monte Carlo sampling (impact parameter, vibrational phases and spatial orientation). The respective maximum impact parameters are, $b_{max}$ = 2.2 and 2.8 Å, which were independently obtained by running small batches of trajectories, until no reactive trajectories were found. Finally, Table S1 lists the QCT input parameters used in the present study.

Next, from the outcome of the independent QCT calculations, T = 298 K and E = 8 kcal mol$^{-1}$, we analyse the product dynamics properties. The reaction cross section is defined as the ratio between the number of reactive ($N_r$) and the total ($N_T$) number of trajectories,

$$\sigma_r(T,E) = \pi b_{\max}^{\ 2} \frac{N_r}{N_T} \qquad \text{(S3)}$$

where the standard error is always <3%. However, the ZPE violation problem (how to deal with reactive trajectories ending with vibrational energy below its ZPE, which is quantum mechanically forbidden) is a serious limitation in QCT calculations and no definitive solutions have been proposed. To address this problem two approaches were used: i) To consider all trajectories independent of the ZPE, and ii) To consider only reactive trajectories where each product, HO and $SiH_3$, presents a vibrational energy above its ZPE, 5.34 and 13.36 kcal mol$^{-1}$, respectively, double zero point energy (DZPE) approach.[s12]

In addition to the reaction cross section, the following product dynamics properties were obtained: relative translational energy between products, scattering angles, vibrational and rotational energies of the HO and $SiH_3$ products and rotational and vibrational actions of the HO diatomic product. The product scattering distribution (velocity vector of the HO product with respect to the incident oxygen atom) is measured as differential cross section, DCS,

$$\frac{d\sigma_r}{d\Omega} = \frac{\sigma_r P(\theta)}{2\pi sin\theta} \qquad (S4)$$

where Ω represents the solid angle, θ the scattering angle and P(θ) the product angular distribution, obtained by a histogram analysis in the range [0,π], which was divided in 18 equal intervals of 10º counting the number of reactive trajectories per interval. Note

that to obtain continuous and smooth functions, the DCSs were fitted using Legendre polynomials.[s13] Obviously, given the classical nature of the QCT calculations, the HO product rotational and vibrational actions are non-integer numbers, and so to pseudo-quantize them, they are rounded to the nearest integer value. Finally, to deal with vibrational quantization two binning approaches were used: i) histogram binning (HB), where all reactive trajectories contribute with the same weight unit, and ii) energy-based Gaussian binning (1GB),[s14,s15] where a Gaussian weight is assigned to each trajectory, i.e., larger weights are related with vibrational energies closer to their quantum values.

## References


s1) G. C. Schatz, B. Amaee and J. N. L. Connor, *J. Chem. Phys*., 1990, **92**, 4893.

s2) D. Troya, R. Z. Pascual and G. C. Schatz, *J. Phys. Chem. A*, 2003, **107**, 10497.

s3) B. C. Garrett and D. G. Truhlar, *J. Am. Chem. Soc*. 1979, 101, 4534.

s4) D. G. Truhlar, A. D. Isaacson and B. C. Garrett, Generalized Transition State Theory. In Theory of Chemical Reaction Dynamics; Baer, M., Ed.; CRC Press: Boca Raton, FL, 1985; Vol. 4, pp 65−137.

s5) C.F. Jackels, Z. Gu and D.G. Truhlar, *J. Chem. Phys.,* 1995, 102, 3188.

s6) G.A. Natanson, B.C. Garrett, T.N. Truong, T. Joseph and D.G. Truhlar, *J. Chem. Phys.* 1991, 94, 7875.

s7) Y.Y. Chuang and D.G. Truhlar, *J. Phys. Chem. A* 1997, 101, 3808.

s8) Y-P. Liu, D. h. Lu, A. Gonzalez-Lafont, D. G. Truhlar and B. C. Garrett, *J. Am. Chem. Soc*. 1993, 115, 7806.

s9) J. Zheng, J.L. Bao, R. Meana-Paneda, S. Zhang, B.J. Lynch, J.C. Corchado,Y.Y. Chuang, P.L. Fast, W.P. Hu, Y.P. Liu, G.C. Lynch, K.A. Nguyen, C.F. Jackles, A. Fernandez-Ramos, B.A. Ellingson, V.S. Melissas, J. Villa, I. Rossi, E.L. Coitiño, J. Pu, T.V. Albu, A. Ratkiewicz, R. Steckler, B. C. Garret, A.D. Isaacson and D.G. Truhlar, POLYRATE-2016-2A, University of Minnesota, Minneapolis, MN, 2016.

s10) X. Hu, W.L. Hase and T. Pirraglia*, J.Comput.Chem*. 1991, 12, 1014.

s11) W.L. Hase, R.J. Duchovic, X. Hu, A. Komornicki, K.F. Lim, D-h. Lu, G.H. Peslherbe, K.N. Swamy, S.R. Vande Linde, A.J.C. Varandas, H. Wang and R.J. Wolf, VENUS96: A General Chemical Dynamics Computer Program, QCPE Bull. 1996, 16, 43.

s12) L. Bonnet and J. C. Rayez*, Chem. Phys. Lett*. 1997, **277**, 183.

s13) D. G. Truhlar and N. C. Blais, *J. Chem. Phys*., 1977, **67**, 1532.

s14) G. Czako and J.M. Bowman, *J. Chem. Phys.* 2009, 131, 244302.

s15) L. Bonnet and J. Espinosa-Garcia, *J. Chem. Phys.* 2010, 133, 164108.

**Table S1**. Input parameters for QCT calculations[a] for the $O(^3P) + SiH_4$ reaction

| Parameter | $O(^3P) + SiH_4$ | Explanation |
|---|---|---|
| Temperature, T | 298 | Temperature (K) |
| $b_{max}$ | 2.2 | Maximum impact parameter (Å) |
| Trajectories | 2 000 000 | Number of trajectories run |
| Reactant vibration | Thermal sampling | $SiH_4$ vibrational energy |
| Reactant rotation | Thermal sampling | $SiH_4$ rotational energy |
| Energy, E | 8.0 | Collision energy (kcal $mol^{-1}$) |
| $b_{max}$ | 2.8 | |
| Trajectories | 2 000 000 | |
| Reactant vibration | Ground-state | |
| Reactant rotation | Thermal sampling | $SiH_4$ rotational energy at 10 K |
| For both T and E | | |
| Si-O distance | 15.0 | Initial and final Si-O separation (Å) |
| ε | 0.1 | Propagation step (fs) |
| Impact parameter, vibrational phases and spatial orientation | Montecarlo sampling | |

a) A more complete explanation of these parameters can be found in the VENUS code manual.[s11]

**Figure S1**

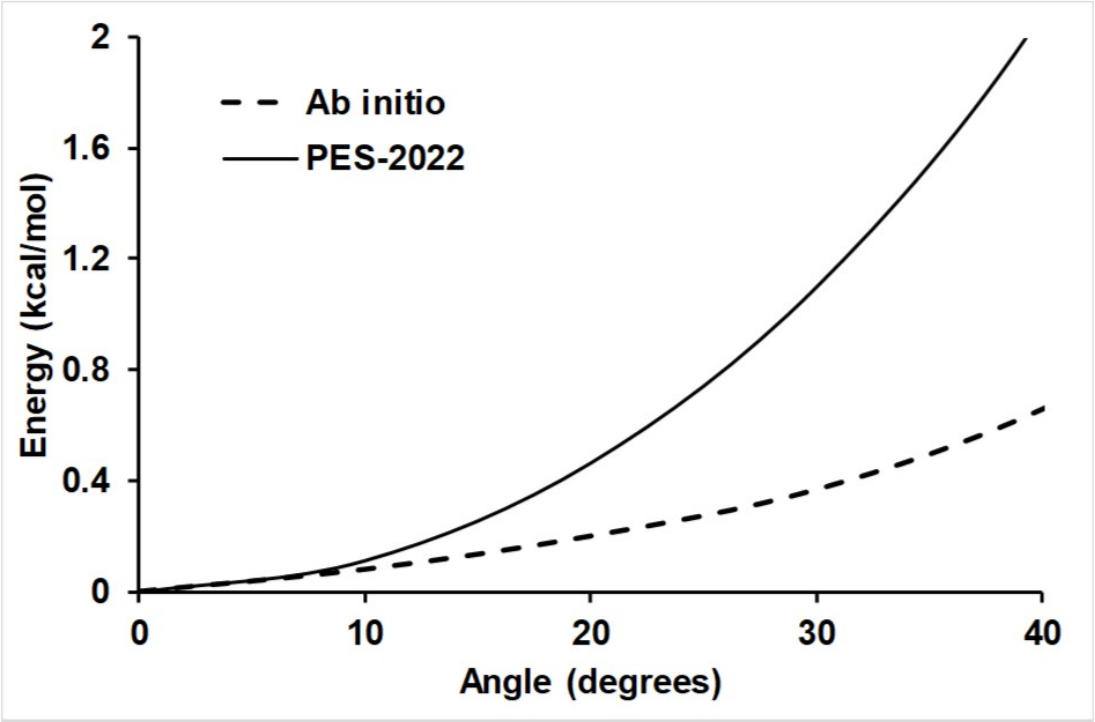


Figure S1. Dependence of energy on the bonding angle in the saddle point, Si-H-O for the PES-2022 (solid line) and the CCSD(T)/cc-pVTZ level (dashed line). The corresponding equilibrium geometry at the saddle point is taken as a reference (level zero).

**Figure S2**

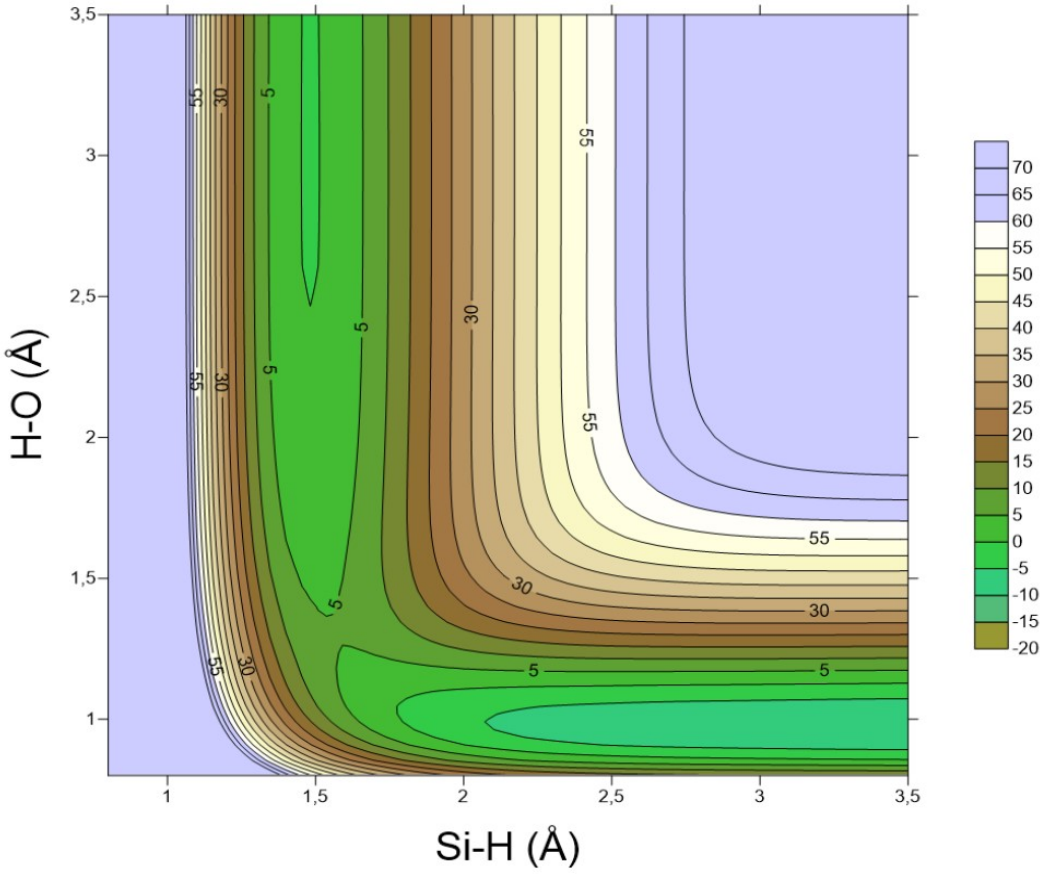


Figure S2. Equipotential contour plot for the $O(^3P)$ + $SiH_4$ reaction using PES-2022. The contour line spacing is also represented. Note that this plot corresponds to a frozen scan, i.e., only the broken (Si-H) and formed (O–H) bonds are varied, while the remaining geometric parameters at the saddle point remain fixed.